6100 J. Med. Chem. 2010, 53, 6100–6111
DOI: 10.1021/jm100507q

Journal of Medicinal Chemistry Article

Non-Peptide Macrocyclic Histone Deacetylase Inhibitors Derived from Tricyclic Ketolide Skeleton

Sandra C. Mwakwari,[†] William Guerrant,[†] Vishal Patil,[†] Shabana I. Khan,[§] Babu L. Tekwani,[§] Zachary A. Gurard-Levin,[∥] Milan Mrksich,[∥] and Adegboyega K. Oyelere*,[†,‡]

[†]*School of Chemistry and Biochemistry, and* [‡]*Parker H. Petit Institute for Bioengineering and Bioscience, Georgia Institute of Technology, Atlanta, Georgia 30332-0400,* [§]*National Center for Natural Products Research and Department of Pharmacology, School of Pharmacy, University of Mississippi, University, Mississippi 38677-1848, and* [∥]*Department of Chemistry and Howard Hughes Medical Institute, University of Chicago, Chicago, Illinois 60637-1511*

Received April 26, 2010

Inhibition of histone deacetylase (HDAC) function is a validated therapeutic strategy for cancer treatment. Of the several structurally distinct small molecule histone deacetylase inhibitors (HDACi) reported, macrocyclic depsipeptides possess the most complex cap groups and have demonstrated excellent HDAC inhibition potency and isoform selectivity. Unfortunately, the development of macrocyclic depsipeptides has been hampered in part because of development problems characteristic of large peptides and the complex reaction schemes required for their synthesis. Herein we report that tricyclic ketolide TE-802 is an excellent mimetic for the peptide backbone of macrocyclic HDACi. Compounds derived from this template are particularly selective against HDACs 1 and 2 with nanomolar inhibitory activity. Interrogation of the association between a subset of these compounds and key HDAC isoforms, using AutoDock, enables a molecular description of the interaction between the HDAC enzyme's outer rim and the inhibitors' macrocyclic cap group that are responsible for compound affinity and presumably isoform selectivity.

Introduction

Histone deacetylase (HDAC[a]) and histone acetyltransferase (HAT) are two functionally opposing enzymes, many of which tightly regulate the chromatin structure and function via sustenance of equilibrium between the acetylated and deacetylated states of histones. By catalyzing the removal of acetyl groups, HDACs induce a condensed chromatin structure resulting in transcription repression, whereas acetylated histones are associated with a more accessible/open chromatin structure and activation of transcription.[1−4] In addition, many non-histone proteins such as tubulin, ERα, p53, HSP 90, NF-YA, and GATA-1 have been found in an acetylated state and may be substrates of HDACs.[5−10] Eighteen human HDAC isoforms are known, and they are subdivided into the classical zinc dependent HDACs comprising classes I, II, and IV and NAD^+ dependent sirtuins, class III enzymes.[9,11,12]

HDAC inhibitors (HDACi) are an emerging class of novel anticancer drugs with a demonstrated ability to arrest proliferation of nearly all transformed cell types, including epithelial (melanoma, lung, breast, pancreas, ovary, prostate, colon, and bladder) and hematological (lymphoma, leukemia, and multiple myeloma) tumors.[13] To date, several classes of small molecule HDACi (fitting a three-motif pharmacophoric model, namely, a zinc-binding group (ZBG), a hydrophobic linker, and a recognition cap group[14] (Figure 1a)) have been reported. Examples include hydroxamic acids such as trichostatin A (TSA), suberoylanilide hydroxamic acid (SAHA) (approved in 2006 by the FDA for the treatment of cutaneous T-cell lymphoma (CTCL)[15,16]), benzamides, short chain fatty acids, electophilic ketones, and cyclic peptides such as FK-228 (romidepsin) which was recently approved by the FDA[17,18] for the treatment of CTCL in patients who have received at least one prior systemic therapy (Figure 1b,c).[19,20] However, most of these drugs nonspecifically inhibit various HDAC isoforms. At the fore of HDAC drug development is the identification of isoform-selective HDACi with the potential for enhanced potency and reduced side effects, compared to the current pan-HDACi. However, these efforts have been so far modestly successful, resulting in only few HDACi that demonstrate partial selectivity.[21,22]

On the other hand, macrocyclic peptide HDACi have the most complex recognition cap group moieties and present an excellent opportunity for the selective modulation of the biological activities of HDACi. Although they possess potent HDAC inhibition activity (nanomolar range), their progress through clinical trials has been slow.[17,18,23] The paucity of clinically effective cyclic-peptide HDACi may be in part due to development problems characteristic of large peptides, most especially poor oral bioavailability. Identification of non-peptide macrocyclic HDACi will offer a new class of macrocyclic HDACi with potentially more favorable druglike properties. Furthermore, this will enhance our understanding of the roles of specific interactions between the enzyme outer rim and inhibitor cap groups in HDACi activity and ultimately aid in the identification of more isoform-selective HDACi.

Recently we reported that non-peptide macrocyclic skeletons derived from 14- and 15-membered macrolides are suitable as surrogates for the cap groups of macrocyclic HDACi (Figure 1d). The resulting HDACi have improved enzyme inhibition potency and isoform-selectivity.[24] Herein, we report

*To whom the correspondence should be addressed. Phone: 404-894-4047. Fax: 404-894-2291. E-mail: aoyelere@gatech.edu.

[a] Abbreviations: HDAC, histone deacetylase; HAT, histone acetyltransferase; HDACi, histone deacetylase inhibitors; HDLP, histone deacetylase-like protein; SAHA, suberoylanilide hydroxamic acid; TSA, trichostatin A; ZBG, zinc-binding group; MALDI, matrix assisted laser desorption/ionization; SAM, self-assembled monolayers.

 Published on Web 07/29/2010

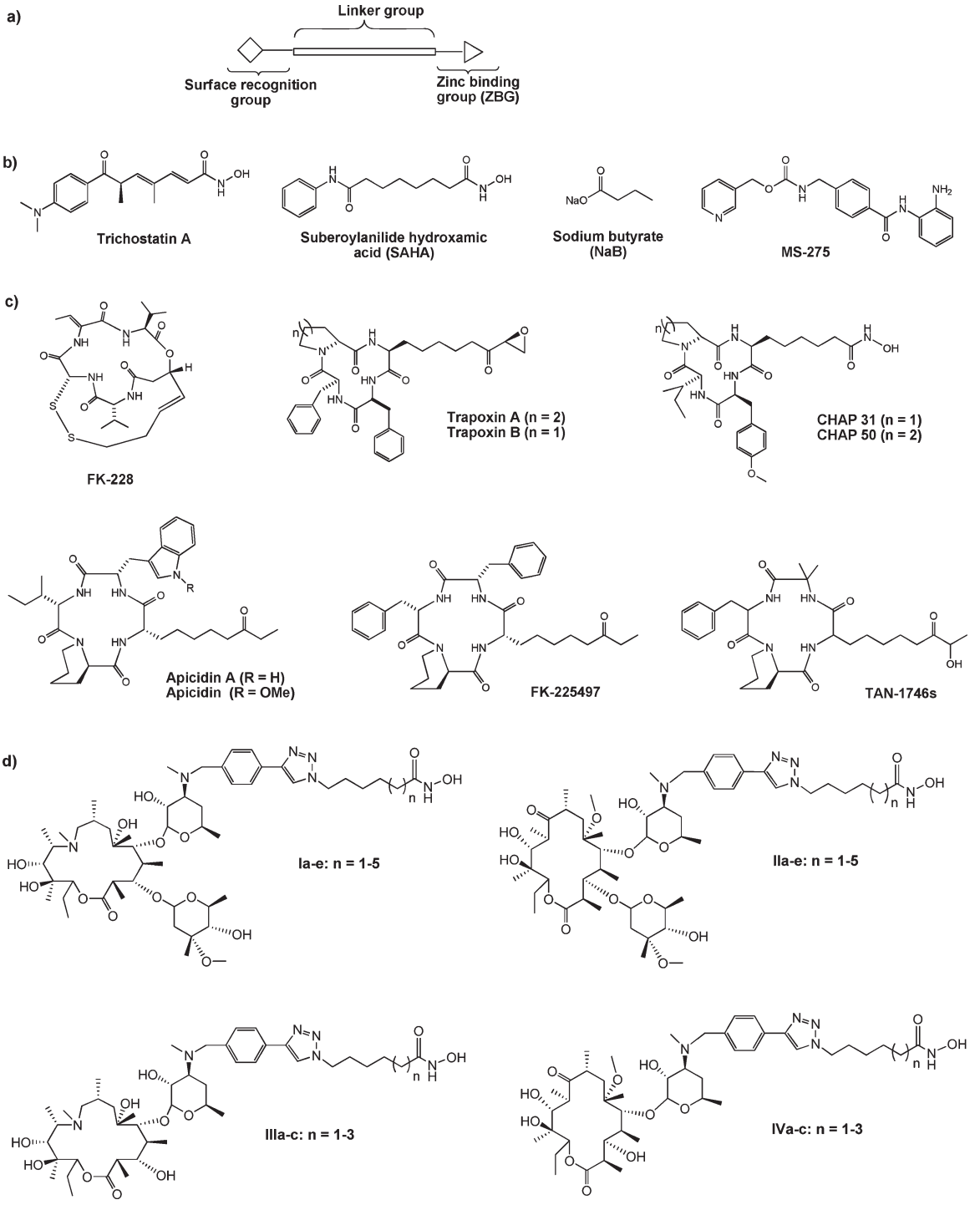

Figure 1. (a) Pharmacophoric model of HDACi and representative examples of (b) acyclic, (c) cyclic peptide, and (d) macrolide-based HDAC inhibitors.

that enhancement of the 14-membered macrolide ring hydrophobicity and rigidity facilitates specific drug interactions with the enzyme's outer rim residues, maximizes HDAC inhibition, and improves drug cytotoxicity against human cancer cell lines. Moreover, these compounds have antiparasitic activities against causative parasites of malaria and leishmaniasis in a manner that reveals structural attributes that confer a specific antiparasitic response.

Results and Discussion

Molecular Docking Analysis. Previous molecular docking studies on HDACi derived from 14- and 15-membered macrolides clarithromycin and azithromycin, respectively, using histone deacetylase-like protein (HDLP), revealed the structural basis for the enhanced activity of these macrocyclic compounds. Either ring system adopted docked orientations that displayed molecular surface complementarities between the macrolide skeleton and the enzyme outer rim.[24] In these docked structures, most of the hydrophobic components of the macrolide ring optimally interact with the hydrophobic residues within HDLP hydrophobic pockets. Common to both ring systems are the vicinal diols at C11 and C12 and at C12 and C13 for clarithromycin and azithromycin, respectively, which have to be accommodated within the enzyme hydrophobic

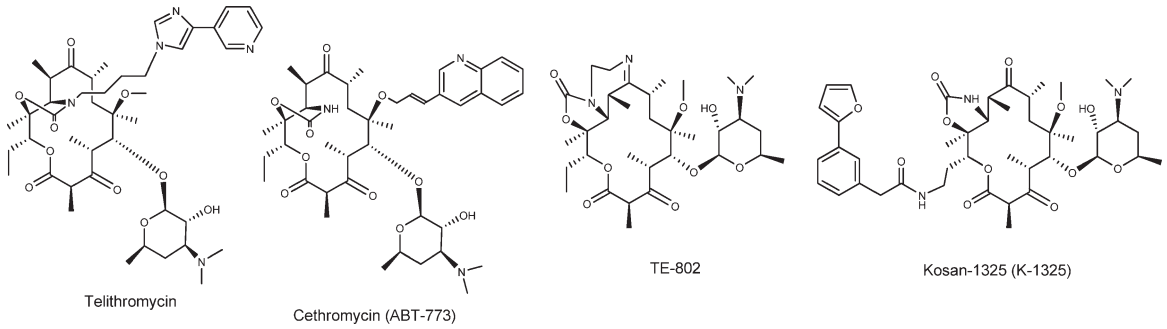

Figure 2. Representative examples of ketolides.

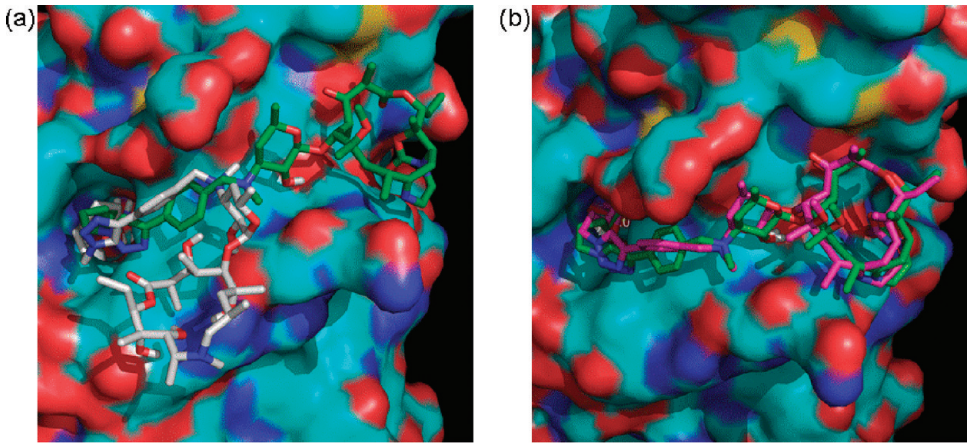

Figure 3. Docked structures of ketolide-derived HDACi at the active site of HDAC1. (a) Superposition of the low energy conformation of **IIIb** (gray) and **15b** (green) revealed the pocket binding preferences of inhibitors at the HDAC1 surface. (b) Relative orientation of the macrocyclic rings of **15a** (pink) and **15b** (green) within the hydrophobic pocket on HDAC1 outer rim.

pocket. We postulated that refinement of the ring hydrophobicity through appropriate modification of the vicinal diols could further modulate the HDAC inhibition of these non-peptide macrocyclic HDACi. In the previous report, we observed that the two macrolide skeletons contributed distinctly to the overall HDAC binding. For 14- and 15-membered macrolides with C_5 and C_6 linkers, the 14-membered compounds are about 2- to 5-fold more potent HDACi than their 15-membered counterparts.[24] On the basis of the foregoing, we focused on the transformation of the 14-membered macrocyclic template.

Conversion of the 14-membered ring vicinal diols to various five-membered carbamates is a common and synthetically tractable approach toward their transformation to relatively more hydrophobic ketolide skeletons (Figure 2).[25−27] The template of ketolide **10** (TE-802),[25] in which the carbamate NH group has been further substituted with a small hydrophobic group that results in a tricyclic ring system, is very attractive in this regard. The rigid template of **10** minimally perturbs the ring within the region of interest while maximizing ring hydrophobicity and should be compatible with the enzyme outer rim hydrophobic pocket. To verify this prospect, we proceeded to interrogate the binding interaction between HDAC1 homology model built from human HDAC2 X-ray structure 3MAX coordinates[28] and the non-peptide macrocyclic hydroxamates **15a**,**b**, derived from the ketolide **10**, using AutoDock as described previously. We focused on the C_5 and C_6 linked compounds **15a**,**b** because these spacer lengths are optimal for the anti-HDAC activity of the previous non-peptide macrocyclic HDACi.[24] Molecular docking analysis revealed that the enhanced hydrophobicity and/or rigidity of the ketolide moiety of the C_5 and C_6 linker compounds **15a** and **15b**, respectively, forced their rings to adopt docked orientations that are distinct from the corresponding macrolide template whose ZBG makes similar interaction with the active site Zn^{2+} ion (Figure 3a). The desosamine sugar 2′-OH group of both **15a** and **15b** is within 1.9 Å of the backbone carbonyl group of Tyr24 with which it could potentially engage in a stabilizing H-bonding interaction (see Supporting Information Figure S1a). Relative to that of **15a**, the ketolide ring of **15b** fits optimally into a hydrophobic pocket on HDAC1 outer rim. The aryl moiety of **15b** is partly stacked on top of His28 that forms the base of a hydrophobic cleft at the entrance to a pocket-like active site (Figure 3b and Supporting Information Figure S1b). The orientation of the aryl moiety enables the C_6-linker methylene group to efficiently present the hydroxamate ZBG to the active site Zn^{2+} ion. To accommodate for the loss of one methylene group and consequently optimally interact with the active site zinc, the ketolide ring of **15a** is slightly lifted out of the pocket while its aryl moiety is twisted, almost perpendicular to the aryl moiety of **15b**, to make a minimal edge contact with His28 at the pocket entrance cleft. In this orientation, **15a** is more solvent exposed relative to **15b** (Figure 3b). The observed disparities in the docked orientations of **15a** and **15b** may have implications on their affinity for the enzyme.

Chemistry. To experimentally test these in silico observations, we synthesized compounds **15a**−**e**. Our proposed synthesis of the requisite compounds involves the intermediacy of 4-ethynylbenzylketolide **9**. We envisioned that **9** could be accessed via two different routes (A and B) whereby the 4-ethynylbenzyl group is introduced early or late in the synthesis

Scheme 1. Synthesis of Tricyclic Ketolide **9** from Clarithromycin **1**

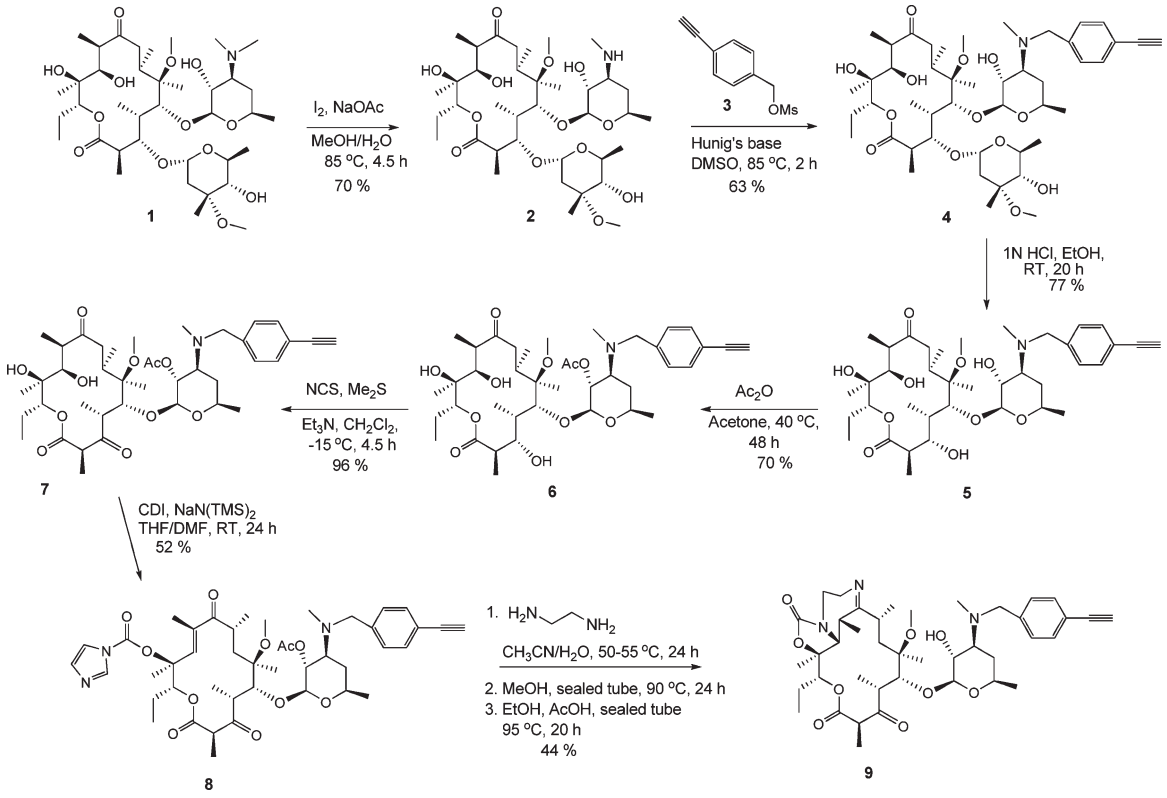

Scheme 2. Synthesis of Tricyclic Ketolide **9** from Ketolide **10**

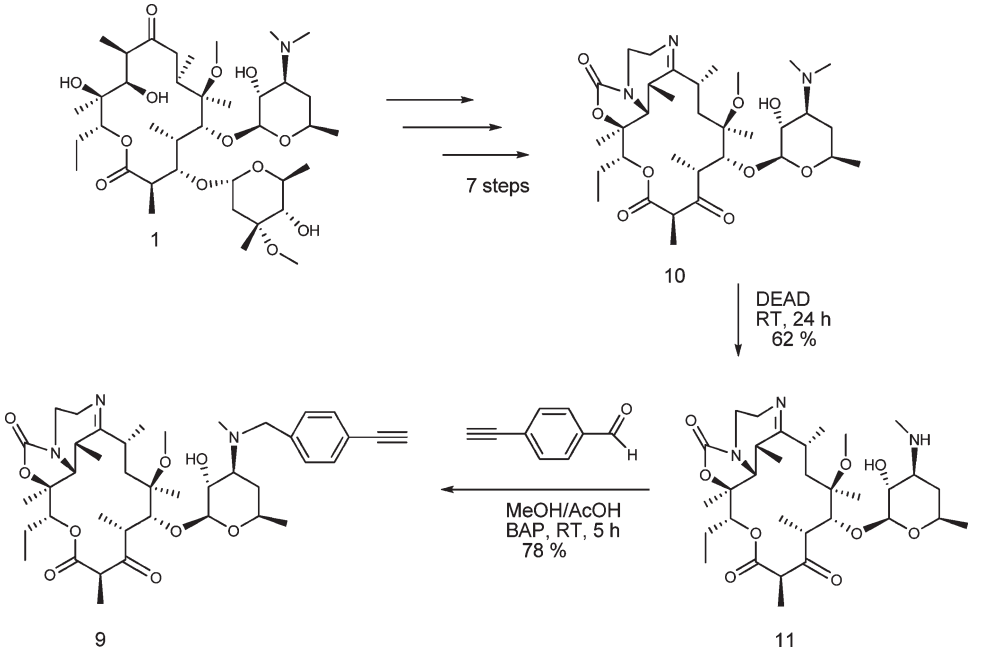

(Schemes 1 and 2, respectively). It is gratifying to note that both routes worked equally well in furnishing intermediate **9**.

Demethylation of clarithromycin **1** under standard conditions gave 3′-desmethyl-clarithromycin **2** in 70% yield.[29] Subsequent alkylation of **2** with 4-ethynylbenzyl methanesulfonate afforded the modified 4-ethynylbenzylclarithromycin **4** which was treated with 1 N HCl to selectively cleave the cladinose sugar and afford compound **5**. It was observed for this reaction step that time was of essence, as longer reaction times led to extensive byproducts formation. Selective acetylation of the 2′-OH group was accomplished by treating an acetone solution of **5** with acetic anhydride at 40 °C for 48 h to give compound **6** in 70% yield. Subsequent oxidation of the 3-hydroxyl group of compound **6** to a 3-keto functional group, under anhydrous conditions with NCS, afforded the ketolide **7** in a near quantitative yield. Treatment of **7** with excess carbonyldiimidazole (CDI) and NaHMDS in a mixture of THF/DMF afforded the 12-carbamoylimidazolide ketolide **8** in 52% yield. Transformation of **8** into the desired

Scheme 3. Synthesis of Triazole-Linked Tricyclic Ketolide Hydroxamates **15**

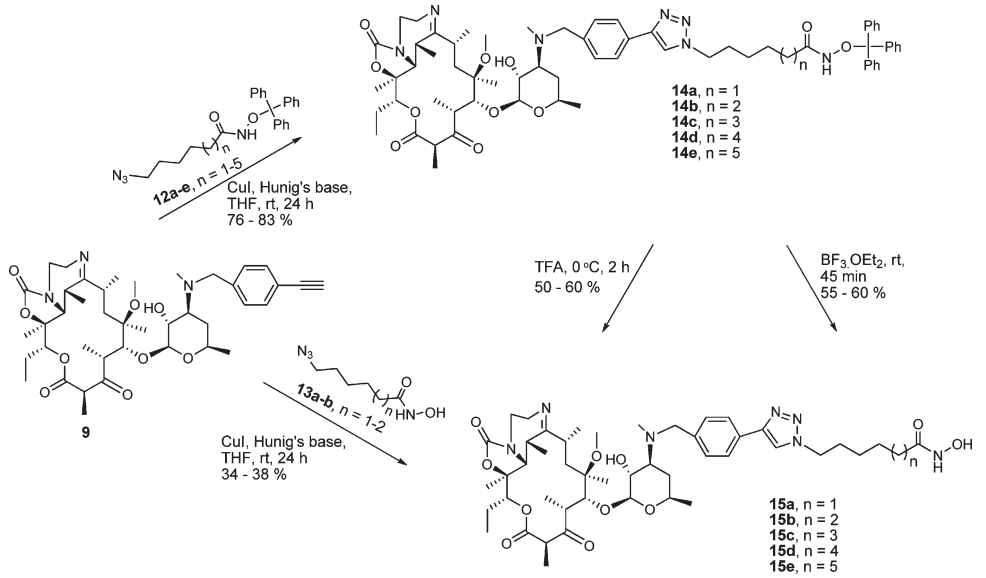

Table 1. HDAC Inhibition Activity (IC_{50}) and Isoform Selectivity of Tricyclic Ketolide-Based HDAC Inhibitors

compd	*n*	nuclear extract (nM)	HDAC8 (nM)	HDAC8/nuclear extract isoform selectivity	HDAC6 (nM)	HDAC6/nuclear extract isoform selectivity
15a	1	7.77	796.2	102.5	1180.1	151.9
15b	2	1.03	544.6	528.7	728.7	707.5
15c	3	104.2	1909.3	18.3	1709.8	16.4
15d	4	163.6	2859.9	17.5	1916.9	11.7
15e	5	208.2	4557.8	21.9	3203.1	15.4
SAHA[a]		65.0	1860.0	29	85.5	1.3

[a] Cited from ref 22.

tricyclic ketolide **9** was achieved in two successive cyclization steps adapting literature procedures.[25] Reaction of imidazolide **8** with ethylenediamine followed by intramolecular Michael addition led to the formation of 11,12-cyclic carbamate. Subsequent intramolecular dehydration completed the cyclization process, affording the desired product **9** in 44% yield (Scheme 1).

Alternatively, intermediate **9** could be directly obtained from **10**. We synthesized **10** from clarithromycin **1** according to a literature procedure.[25,26,30,31] Subsequent N-demethylation of **10** using diethyl azodicarboxylate (DEAD) gave the expected *N*-desmethyl ketolide **11** in 62% yield.[31] Reductive amination of **11** with 4-ethynylbenzaldehyde using borane−pyridine complex (BAP) afforded the requisite intermediate **9** in 78% yield (Scheme 2).

The final transformation of **9** to **15a**−**e** was uneventful (Scheme 3). Copper(I) catalyzed cycloaddition reaction[24] of **9** with *O*-trityl protected azidohydoxamate analogues **12a**−**e** afforded the 1,2,3-triazole linked derivatives **14a**−**e**. Deprotection of the trityl group of **14a**−**e** with TFA gave the desired products **15a**−**e** in good yields. A similar outcome was obtained when trityl group deprotection was effected with $BF_3 \cdot OEt_2$. Alternatively, the desired hydroxamates could be obtained through direct copper(I) catalyzed cycloaddition between unprotected azidohydroxamates **13** and alkyne **9**, according to our published protocol.[24]

HDACi Activity and Selectivity of 15a−**e.** We first tested compounds **15a**−**e** for their HDAC inhibitory activity (Table 1) against HeLa cell nuclear extract (which contains primarily HDACs 1 and 2), HDAC6, and HDAC8 using the Fluor de Lys assay kit (Enzo Life Sciences, Inc.).[32−34] Results show a linker-length-dependent anti-HDAC activity which peaked with compound **15b**, an analogue having six methylene linkers separating the triazole ring from the zinc binding hydroxamic acid group (Table 1). Compound **15b** potently inhibits the deacetylase activity of HeLa nuclear extract with a single digit nanomolar IC_{50}. Although compound **15a** (analogue having five methylene linkers) also has nanomolar inhibition activity against the nuclear extract, it is nevertheless over 7-fold worse than **15b**. The HDAC inhibition profiles of **15a** and **15b** paralleled those we previously reported for the macrolide-derived HDACi of the same linker lengths.[24] Additionally, this result is in close agreement with the in silico prediction using HDAC1 which revealed that **15b** adopted a docked orientation with a better fit with the enzyme outer rim hydrophobic pocket (Figure 3b). The affinity of **15a** for the enzyme could be compromised by the solvent exposure of its macrocyclic ring and the shortness of its linker region relative to that of **15b**. These shortcomings in the docked structure of **15a** may explain the 7-fold enhanced anti-HDAC activity of **15b** relative to **15a**.

Compounds **15c**−**e**, analogues having longer methylene linkers than those of **15b**, show a progressive reduction in anti-HDAC activity with the increase in linker length (Table 1). We then performed further molecular docking analyses on HDAC1 with the goal of shedding more light on the chain length dependence reduction in the anti-HDAC activities of these longer chain compounds. We observed that these longer linker compounds adopted various docked orientations which progressively extruded the ketolide ring from the outer rim pocket into

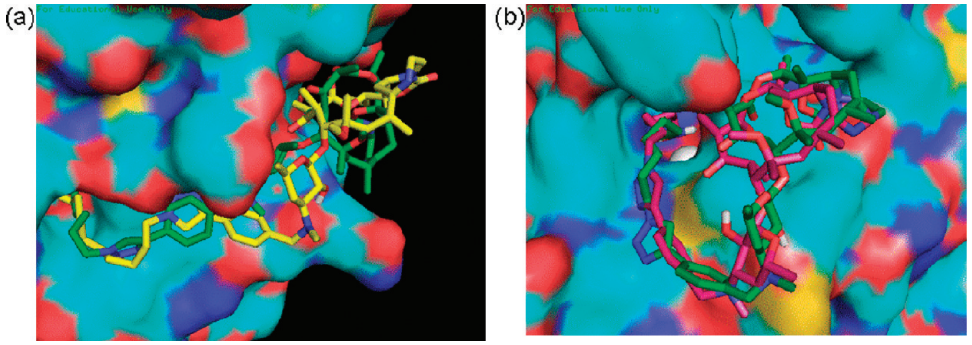

Figure 4. Comparison of the orientations of (a) the C_6-linker compound **15b** (green) and C_9-linker compound **15e** (yellow) at the outer rim of HDAC1 and (b) the C_5-linker compound **15a** (pink) and C_6-linker compound **15b** (green) at the outer rim of HDAC8.

solvent exposed regions on the enzyme surface. Compound **15e**, the analogue with the longest methylene linker in the series herein disclosed, made the least interaction with the enzyme outer rim (Figure 4a). The observed extrusion of the macrocyclic ring from the enzyme surface as the methylene linker length increases could compromise the compounds' affinity for the enzyme. These in silico observations provide a plausible structural basis for the observed chain length dependence attenuation of the anti-HDAC activities of these ketolide-derived HDACi.

To obtain evidence for the HDAC isoform selectivity, we tested all triketolide HDACi herein described against HDAC6 and HDAC8 using the Fluor de Lys assay. Compared to SAHA, compounds **15a** and **15b** are more selective for the nuclear extract (HDACs 1 and 2) with selectivity indices comparable to those of their 14-membered macrolide congeners.[24] Compounds **15c**−**e** are less selective for either HDAC isoform compared to **15a**,**b**. However, **15c**−**e** have improved HDAC6 and comparable HDAC8 isoform selectivity relative to SAHA (Table 1). The linker length dependent dissipation of HDAC isoform selectivity could also be due to the relief of the attractive interactions between the ketolide macrocycle and the enzyme hydrophobic cleft, a concomitant effect of the increase in compounds' spacer length. HDAC8 could be particularly sensitive to changes in linker length because it has a much shallower active site pocket relative to HDAC1.[35] To gain insight into the structural basis of the observed isoform selectivity, we performed molecular docking analysis on the HDAC8 structure reported by Somoza et al.[35] In contrast to their docked structures on HDAC1, the orientations of **15a** and **15b** that enable interaction of the ZBG with the active site Zn^{2+} ion are those that adopted a closed conformation (Figure 4b). In this conformation, the macrolactonic ring of either compound is nestled atop the entrance to the enzyme active site while the desosamine sugar, the triazolylaryl moiety, and a portion of the methylene linker are lifted off the enzyme surface and wrapped back under the macrolactonic ring to enable the ZBG to interact with the Zn^{2+} ion at the base of a shallow active site pocket. This closed conformation is inaccessible to **15e**, the analogue with the longest methylene linkers in the series herein disclosed. Instead, **15e** adopted a conformation in which its macrocyclic moiety is flanged into a distinct solvent exposed patch on the enzyme surface to give its long linker moiety enough room to present the ZBG to the enzyme active site (see Supporting Information Figure S1c). Analyses of X-ray data have revealed significant inhibitor specific changes in the enzyme active site topology of HDAC8.[35] It is therefore possible that the observed HDAC1 isoform selectivity may be partly due to the inability of these ketolide based HDACi to efficiently induce active site conformational changes that facilitate HDAC8 specific inhibitor association with the enzyme active site.[36]

Recent studies have shown that the use of fluorescently labeled substrates can perturb enzyme activity and the effect of inhibitors and activators on the deacetylases.[37,38] In one example, the discovery that resveratrol and various analogues activate the deacetylase sirtuin 1 (SIRT1) was found to be an artifact of the fluorescent assay.[39] Indeed, many recommended Fluor de Lys substrates have been shown not to be active toward their corresponding enzymes, including HDAC8, absent the fluorophore.[40,41] In light of these data, we sought to validate that compounds **15a**−**e** do inhibit HDAC8 using the label-free SAMDI mass spectrometry assay.

The SAMDI technique, wherein self-assembled monolayers (SAM) of alkanethiolates on gold are analyzed by matrix assisted laser desorption/ionization (MALDI) mass spectrometry, has been used to characterize many biochemical activities, including the deacetylase enzyme family.[41−43] The SAMDI assay is also amenable to analysis of homogeneous reactions, as the substrates are immobilized to the SAMs after the reaction has been terminated.[44] We employed the SAMDI technique to measure the inhibition constant (K_i) of compounds **15a**−**e** against HDAC8 using a previously identified preferred HDAC8 substrate, Ac-GRK^{Ac}FGC-NH_2.[41]

In the first example, the reactions were set up in a 96-well plate with 1 μM HDAC8 and varying concentrations of substrate (5, 10, 25, and 50 μM) and inhibitor **15b** (0, 50, 100, 250, and 500 nM). The reactions were stopped at different time points and applied to arrays of gold circles presenting maleimide-terminated SAMs to immobilize the substrate via Michael addition of the cysteine thiol with maleimide. SAMDI spectra were then acquired for each reaction, and a shift of m/z 42 is indicative of a deacetylation reaction (Supporting Information Figure S1). The amount of product formed was plotted over time for each reaction condition to get the initial rates of reaction. A Dixon plot ($1/v$ vs [I]) shows lines corresponding to different substrate concentrations that intersect around 200 nM, which is the K_i for compound **15b** (Figure 5a). We then measured the K_i for the remaining compounds and found that **15b** has the highest affinity for HDAC8. Consistent with the in silico data, we observed a weak affinity for compound **15a** for HDAC8. The K_i values for **15c**−**e** are rather comparable (Figure 5b), yet do mimic the trend observed with the fluorescent assay that as the length of the hydroxamic acid linker increases, the inhibitor affinity decreases. Finally, we note that while we observe a similar inhibition pattern with **15a**−**e** using the two assays, there is a disparity in the absolute magnitude of the inhibition constants. This is anticipated because of the

(a)

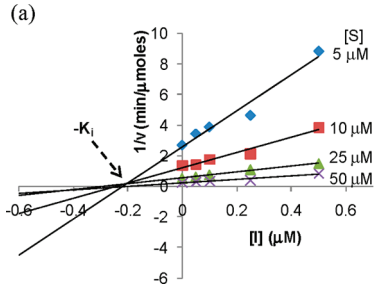

(b)

Inhibitor	K_i (nM)
15a	1100
15b	210
15c	580
15d	620
15e	825

Figure 5. Determination of K_i for compounds **15a**−**e** using SAMDI mass spectrometry: (a) Dixon plot of compound **15b**; (b) K_i values for compounds **15a**−**e** as determined by SAMDI.

Table 2. Antiproliferative Activity (μM) of Tricyclic Ketolide-Based HDAC Inhibitors

compd	*n*	DU-145 (μM)	A549 (μM)	MCF-7 (μM)	Hs1.Lu normal lung fibroblast (μM)
15a	1	1.64	1.17	1.26	>10
15b	2	0.82	0.66	0.75	>10
15c	3	3.70	1.64	1.35	>10
15d	4	3.89	2.48	2.56	>10
15e	5	4.83	2.81	3.68	>10

nature of each assay (including the use of either a labeled or unlabeled substrate) and the parameters that were measured to compare inhibitor potency.

Encouraged by the in vitro HDAC inhibition results, we studied the effect of **15a**−**e** on the viability of three representative cancer cell lines (prostate (DU-145), lung (A549), and breast cancer (MCF-7)) and a nontransformed cell (human lung fibroblast cell (Hs1.Lu)). We included a nontransformed cell line in our investigation in order to obtain evidence for compound selective toxicity. Drug concentrations necessary for 50% inhibition of cell viability (EC_{50}) were quantitatively measured using MTS colorimetric assay as we previously described.[24,45] Table 2 shows the EC_{50} values of each compound. Compounds **15a**−**e** inhibit the proliferation of all transformed cells studied with antiproliferative activity that closely matched their in vitro anti-HDAC activity. Specifically, compound **15b** has the most potent antiproliferative activity with high nanomolar efficacy against all three cancer cell lines. Moreover, none of the compounds show any discernible toxicity against normal Hs1.Lu cells at drug concentrations in excess of 10 μM (Table 2). These data showed that the triketolide hydroxamates reported here are selectively toxic to the transformed cells, a trait that tracks with those of many HDACi.

Rapidly growing eukaryotes including the human pathogenic apicomplexan protozoans and trypanosomatids, such as the causative agents of malaria and leishmaniasis, respectively, have been shown to be responsive to HDACi.[46−50] These earlier observations demonstrate HDACs as promising targets in the fight against the often fatal diseases caused by these parasites. However, the structure−activity relationship (SAR) of the antimalarial and antileishmanial activities of HDACi is not entirely clear. To further profile the biological activities of these triketolide HDACi, we investigated their antiparasitic activities against *Plasmodium falciparum* and *Leishmania donovani*, the causative parasites of human malaria and leishmaniasis, respectively.

The antimalarial activities of compounds **15a**−**e** closely paralleled their anti-HDAC activity against HeLa nuclear extract HDAC. They potently inhibit the proliferation of both the sensitive and resistant strains of *P. falciparum* with IC_{50} ranging from 0.12 to 1.5 μg/mL (Table 3). Again, **15b** has the most potent antimalarial activity, which is between 2- to 4-fold more potent than the control compound SAHA. Moreover, **15b** is several-fold more selectively toxic to either strains of *P. falciparum* compared to SAHA. This result suggests that the parasite HDACs could be one of the compound intracellular targets. To obtain direct evidence for the involvement of *P. falciparum* HDACs as one of the potential intracellular targets for these compounds, we investigated their effects on the activity of *P. falciparum* HDAC1 (pf-HDAC1).[50] All the compounds demonstrate inhibitory activity against pf-HDAC1 with IC_{50} values that followed a similar pattern as their activity against the HeLa nuclear extract HDAC (Table 4). The anti pf-HDAC1 activity of compound **15b**, the most potent in this series, is about 3-fold enhanced relative to the previously reported macrolide HDACi chemotypes with the same linker length.[50] The enhanced anti-pf-HDAC1 activity of **15b** could be due to a better fit to the enzyme afforded by its rigid tricyclic ring. Overall, this result confirms that these ketolide based HDACi partly derived their antimalarial activity through intracellular inhibition of pf-HDAC1 activity.

Interestingly however, compounds **15a**,**b** are devoid of antileishmanial activity against the promastigote stage of *L. donovani* while compounds **15c**−**e** have moderate to good activity that peaks with **15e**, the analogue with the longest methylene spacer in the series disclosed in this manuscript (Table 3). This result is in contrast to the antimalarial activity that mirrors compound anti-HDAC activity, and it may have implications in the organization of the active sites of the relevant *P. falciparum* and *L. donovani* HDAC isozymes. We have observed a similar methylene spacer-length dependence in the antileishmanial activity of macrocyclic HDACi derived from 14- and 15-membered macrolides.[46,50] The foregoing observations further support the suitability of HDAC inhibition as a viable therapeutic strategy to curb infections caused by apicomplexan protozoans and trypanosomatids.

Conclusion

We report that tricyclic ketolide is an excellent mimetic for the peptide backbone of macrocyclic HDACi. The tricyclic ketolide herein described has a rigid hydrophobic skeleton that, as we confirmed by molecular docking analysis, favorably interacts with the HDAC enzyme's outer rim groups, thereby resulting in enhanced HDAC inhibition profile. Compounds derived from this template are particularly selective against HeLa nuclear extract HDACs 1 and 2 with nanomolar inhibitory activity and have improved drug cytotoxicity against human cancer cell lines. Many of these compounds have superior antiparasitic activities against causative parasites of malaria and leishmaniasis compared to clinically useful SAHA. The pattern of the antimalarial and antileishmanial activities of these compounds reveals structural attributes that confer a specific antiparasitic response. Finally, ketolides, like their 14- and 15-membered macrolide counterparts, have selective tissue/cell distribution profiles. For example, ketolides have been reported to exceptionally accumulate in the phagocytes, in particular, human polymorphonuclear neutrophils (PMNs) and other phagocytic and epithelial cell lines.[51] Therefore, these ketolide derived HDACi could find application in targeting tumor-associated

Table 3. In Vitro Antileishmanial (μg/mL) and Antimalarial (μg/mL) Activities of Tricyclic Ketolide-Based HDAC Inhibitor Derivatives[a]

		antileishmanial activity[b]		antimalarial activity[c]			
compd	*n*	IC_{50} (μg/mL)	IC_{90}(μg/mL)	*Plasmodium falciparum* (D6 clone) IC_{50} (μg/mL)	*Plasmodium falciparum* (W2 clone) IC_{50} (μg/mL)	cytotoxicity (VERO)[c] IC_{50}(μg/mL)	SI D6 (W2)
15a	1	NA	NA	0.897 ± 0.198	1.789 ± 0.254	NC	>5.3 (>2.68)
15b	2	NA	NA	0.137 ± 0.027	0.133 ± 0.027	NC	>35.0 (>36.0)
15c	3	19.7 ± 2.4	35.8 ± 4.4	1.317 ± 0.231	1.475 ± 0.244	NC	>3.6 (>3.3)
15d	4	14.9 ± 1.7	32.3 ± 3.1	1.296 ± 0.129	1.376 ± 0.079	NC	>3.7 (>3.5)
15e	5	4.8 ± 0.5	23.7 ± 2.4	1.195 ± 0.058	0.897 ± 0.025	NC	>4.0 (>5.3)
chloroquine		NT	NT	0.012 ± 0.002	0.147 ± 0.018	NT	NT
artemisinin		NT	NT	0.0066 ± 0.0007	0.0091 ± 0.0011	NT	NT
pentamidine		1.17 ± 0.25	2.45 ± 0.34	NT	NT	NT	NT
amphotericine B		0.079 ± 0.012	0.395 ± 0.054	NT	NT	NT	NT
SAHA		21.5 ± 3.51	51.7 ± 8.1	0.279 ± 0.077	0.392 ± 0.045	1.375 ± 0.255	4.9 (3.5)

[a] NA = not active up to highest concentration tested. NC = not cytotoxic up to the highest concentration tested. NT = not tested. SI = selectivity index (IC_{50}(Vero)/IC_{50}). [b] Maximum tested concentration = 40 μg/mL. [c] Maximun tested concentration = 4.8 μg/mL.

Table 4. In Vitro Inhibition of pf-HDAC1 by Tricyclic Ketolide-Based HDACi

compd	*n*	IC_{50} (nM)
15a	1	36 ± 2.9
15b	2	10 ± 0.5
15c	3	40 ± 1.8
15d	4	290 ± 16
15e	5	304 ± 17
SAHA		130 ± 9.2

macrophages and further clarify the roles of HDACi in the inhibition of macrophage migration inhibitory factor (MIF) gene, a phenomenon that has been suggested to be an essential part of their antitumorigenic effects.[52]

Experimental Section

Materials and Methods. All commercially available starting materials were used without further purification. Clarithromycin **1** was purchased from Greenfield Chemical. 4-Ethynylbenzyl alcohol, ethyl 6-bromohexanoate, ethyl 7-bromoheptanoate, 8-bromooctanoic acid, and methyl 10-bromodecanoate were purchased from Sigma Aldrich. 9-Bromononanoic acid was purchased from Karl Industries Inc. Reaction solvents were either high performance liquid chromatography (HPLC) grade or American Chemical Society (ACS) grade and used without further purification. HDAC fluorimetric assay kit and recombinant HDACs were procured from Enzo Life Sciences, BIOMOL International, PA. Analtech silica gel plates (60 F_{254}) were used for analytical TLC, and Analtech preparative TLC plates (UV 254, 2000 μm) were used for purification. UV light and anisaldehyde/iodine stain were used to visualize the spots. Silica gel (200−400 mesh) was used in column chromatography. Nuclear magnetic resonance (NMR) spectra were recorded on a Varian-Gemini 400 magnetic resonance spectrometer. ^{1}H NMR spectra were recorded in parts per million (ppm) relative to the peak of $CDCl_3$, (7.24 ppm). ^{13}C spectra were recorded relative to the central peak of the $CDCl_3$ triplet (77.0 ppm) and were recorded with complete heterodecoupling. High-resolution mass spectra were recorded at the Georgia Institute of Technology mass spectrometry facility in Atlanta. Melting points were recorded uncorrected on a MEL-TEMP II apparatus. HPLC assays were performed on a Beckman Coulter instrument using a Phenomenex RP C-18 column (250 mm × 4.6 mm), eluting with solvent A (0.1% formic acid/acetonitrile) and solvent B (0.1% formic acid/water) at a gradient of 5−50% over 30 min, with detection at 251 nm and a flow rate of 1 mL/min. Sample concentrations were 250 μM, injecting 5 μL. 3′-Desmethylclarithromycin **2**, 4-ethynylbenzylclarithromycin **4**, descladinose-4-ethynylbenzylclarithromycin **5**, and azidoalkylhydroxamic acid (**13a**,**b**) were synthesized as we previously reported.[24] Azido-*O*-trityl alkylhydroxamate derivatives (**12a**−**e**) were synthesized by adapting literature protocol.[46]

2′-*O*-Acetyldescladinose-4-ethynylbenzylclarithromycin (6). To a solution of descladinose-4-ethynylbenzylclarithromycin **5** (3.80 g, 5.50 mmol) in acetone (20 mL) was added Ac_2O (0.62 g, 6.00 mmol), and the resulting mixture was stirred at 40 °C for 36 h. The reaction mixture was diluted with EtOAc (100 mL) and washed with aqueous $NaHCO_3$ (70 mL) and saturated brine (70 mL). Purification on silica column (6:1 CH_2Cl_2/acetone) afforded 2.8 g (70%) of the title compound as a yellowish solid. ^{1}H NMR ($CDCl_3$, 400 MHz) δ 0.80 (3H, t, J = 7.2 Hz), 0.90 (3H, d, J = 7.2 Hz), 1.08−1.47 (12H, m), 1.58 (6H, s), 1.63−2.05 (7H, m), 2.08 (3H, s), 2.16 (3H, s), 2.42−2.80 (3H, m), 2.92 (3H, s), 2.94−3.00 (1H, m), 3.03−3.68 (3H, m), 3.79 (2H, s), 3.94 (1H, s), 4.08 (1H, m), 4.54 (1H, d, J = 8.0 Hz), 4.80 (1H, m), 5.15 (1H, dd, J = 11.6, 2.4 Hz), 7.17 (2H, d, J = 8.4 Hz), 7.38 (2H, d, J = 8.0 Hz); ^{13}C NMR ($CDCl_3$, 100 MHz) δ 8.0, 10.7, 12.8, 15.5, 16.4, 18.1, 19.5, 21.3, 21.5, 21.6, 31.1, 31.9, 36.0, 37.0, 37.5, 38.7, 44.3, 45.7, 50.0, 58.4, 62.5, 68.9, 69.8, 71.6, 74.4, 76.9, 77.0, 77.8, 78.1, 81.3, 83.9, 99.9, 120.7, 128.4, 132.2, 141.1, 170.1, 174.9, 221.2; HRMS (FAB, mnba) calcd for $[C_{40}H_{61}NO_{11} + H]^+$ 732.4323, found 732.4311.

2-Oxo-2′-*O*-acetyldescladinose-4-ethynylbenzylclarithromycin (7). Methyl sulfide (1.42 g, 22.80 mmol) was added to a mixture of *N*-chlorosuccinimide (2.61 g, 19.50 mmol) and CH_2Cl_2 (10 mL) while maintaining the temperature at −15 °C. Compound **6** (10.0 g, 13.7 mmol) dissolved in CH_2Cl_2 (50 mL) was added to the reaction flask, followed by Et_3N (1.56 g, 15.4 mmol) and stirred at −15 °C for 4.5 h. The reaction mixture was poured into EtOAc (350 mL) and 0.5 N aqueous NaOH (250 mL). The organic layer was separated, washed with saturated brine (250 mL), and dried over Na_2SO_4. Solvent was evaporated off and the crude was purified on silica column (2:3:0.1 EtOAc/hexane/Et_3N) to afford 9.54 g (96%) of the title compound as an off-white solid. ^{1}H NMR ($CDCl_3$, 400 MHz) δ 0.80−0.86 (6H, m), 1.09−1.57 (12H, m), 1.58 (6H, s), 1.62−2.02 (7H, m), 2.05 (3H, s), 2.15 (3H, s), 2.44−2.80 (2H, m), 2.92 (3H, s), 2.95−3.00 (1H, m), 3.05−3.66 (4H, m), 3.80 (1H, q, J = 14.0, 6.8 Hz), 3.89 (1H, s), 4.12 (1H, m), 4.38 (1H, d, J = 8.0 Hz), 4.79−4.83 (1H, m), 5.14 (1H, dd, J = 11.2, 2.0 Hz), 7.16 (2H, d, J = 7.6 Hz), 7.38 (2H, d, J = 7.6 Hz); ^{13}C NMR ($CDCl_3$, 100 MHz) δ 10.8, 12.4, 14.4, 14.5, 16.5, 17.9, 19.6, 21.3, 21.5, 31.3, 36.9, 37.6, 39.2, 45.1, 46.3, 49.7, 51.1, 58.5, 62.5, 69.2, 69.6, 71.5, 74.1, 77.0, 77.1, 77.2, 78.1, 83.9, 101.1, 120.7, 128.5, 132.2, 140.9, 169.6, 170.0, 205.7, 221.1; HRMS (FAB, mnba) calcd for $[C_{40}H_{59}NO_{11} + H]^+$ 730.4166, found 730.4132.

12-Carbamoylimidazole Ketolide (8). To a suspension of **7** (1.50 g, 2.06 mmol) in a mixture of anhydrous THF (20 mL) and anhydrous DMF (7 mL) was added CDI (1.30 g, 8.20 mmol)

followed by a solution of 1.0 M $NaN(TMS)_2$ in THF (2.60 mL, 2.60 mmol) over 75 min, and the resulting mixture was stirred at room temperature for 24 h. The reaction mixture was diluted with EtOAc (50 mL), washed with aqueous $NaHCO_3$ (20 mL) and saturated brine (20 mL), and dried over Na_2SO_4. Solvent was evaporated off and the crude was purified on silica column (3:2:0.1 EtOAc/hexane/Et_3N) to yield 52% (0.86 g) of the title compound. ^{1}H NMR ($CDCl_3$, 400 MHz) δ 0.91 (3H, t, 7.6 Hz), 1.09 (3H, d, J = 7.2 Hz), 1.14−1.50 (9H, m), 1.80 (3H, s), 1.83 (3H, s), 1.56−1.94 (7H, m), 2.00 (3H, s), 2.05 (3H, s), 2.12 (3H, s), 2.64−2.80 (1H, m), 3.02 (3H, s), 2.95−3.70 (4H, m), 3.73 (1H, q, J = 14.0, 6.8 Hz), 4.10−4.06 (2H, m), 4.30 (1H, d, J = 7.6 Hz), 4.77−4.80 (1H, m), 5.68 (1H, dd, J = 11.2, 2.0 Hz), 6.77 (1H, s), 7.03 (1H, s), 7.16 (2H, d, J = 7.6 Hz), 7.36 (3H, m), 8.06 (1H, s); ^{13}C NMR ($CDCl_3$, 100 MHz) δ 10.7, 13.5, 14.4, 15.2, 19.1, 20.4, 21.1, 21.2, 21.5, 22.8, 31.2, 36.8, 47.6, 50.5, 51.2, 58.5, 60.6, 62.8, 69.3, 71.6, 78.7, 83.9, 84.7, 117.3, 120.7, 128.4, 131.1, 132.2, 137.3, 138.8, 140.9, 146.2, 169.1, 169.8; HRMS (FAB, mnba) calcd for $[C_{44}H_{59}N_3O_{11} + H]^+$ 806.4228, found 806.4210.

4-Ethynylbenzyltricyclic Ketolide (9). Protocol A. To a solution of **8** (0.60 g, 0. 74 mmol) in CH_3CN (10 mL) and H_2O (1 mL) was added ethylenediamine (0.44 g, 7.40 mmol), and the mixture was heated in a sealed tube at 50−55 °C for 24 h. Solvent was evaporated off and the reaction mixture partitioned between H_2O (15 mL) and CH_2Cl_2 (20 mL) and separated. The organic layer was washed with saturated brine (20 mL), dried over Na_2SO_4, and solvent was evaporated off in vacuo. The crude product was dissolved in anhydrous MeOH (15 mL) and heated at 90 °C in a sealed tube for 24 h. MeOH was evaporated and the product purified on silica column (EtOAc/Et_3N 12:0.1) to give 0.27 g (48%) of the intermediate product. EtOH (6 mL) and AcOH (0.043 g, 0.71 mmol) were added to the pure intermediate product (0.27 g, 0.34 mmol), and the mixture was heated at 95 °C in a sealed tube for 20 h. The reaction mixture was suspended in dilute NH_4OH (10 mL) and CH_2Cl_2 (15 mL) and the organic layer separated, washed with saturated brine (10 mL), and dried over Na_2SO_4. Purification on silica column (EtOAc/MeOH/Et_3N 10:0.5:0.05) afforded 0.24 g (92%), 44% overall yield of compound **9**.

Protocol B: Reductive Amination. A solution of **11** (0.20 g, 0.32 mmol) and 4-ethynylbenzaldehyde (0.21 g, 1.60 mmol) in MeOH (4 mL) and acetic acid (37 μL, 0.64 mmol) was stirred for 30 min at room temperature. Borane−pyridine complex (80 μL, 0.64 mmol) was added and the mixture stirred for 5 h. The mixture was diluted with EtOAc (20 mL) and washed with saturated $NaHCO_3$ (20 mL) and saturated brine (20 mL). The organic layer was dried over Na_2SO_4, concentrated in vacuo, and purified by preparative TLC (12:1 CH_2Cl_2/MeOH) to afford 0.18 g (78%) of compound **9** as a creamish solid. ^{1}H NMR ($CDCl_3$, 400 MHz) δ 0.80 (3H, t, J = 7.2 Hz), 1.00 (3H, d, J = 6.8 Hz), 1.14−1.55 (12H, m), 1.30 (3H, s), 1.43 (3H, s), 1.60−1.96 (6H, m), 2.12 (3H, s), 2.45−2. 95 (6H, m), 3.03 (3H, s) 3.23−3.43 (4H, m), 3.64−3.78 (4H, m), 3. 94 (1H, m), 4.16 (1H, d, J = 8.4 Hz), 4.25 (1H, d, J = 7.6 Hz), 4.90 (1H, d, J = 10.0 Hz), 7.18 (2H, d, J = 8.0 Hz), 7.39 (2H, d, J = 7.2 Hz); ^{13}C NMR ($CDCl_3$, 100 MHz) δ 10.6, 11.1, 13.0, 14.6, 16.6, 19.3, 19.8, 21.4, 22.3, 29.7, 36.5, 37.1, 38.7, 42.5, 43.0, 48.3, 49.3, 49.7, 51.4, 57.6, 60.1, 65.6, 69.7, 70.5, 76.7, 78.7, 79.4, 81.7, 83.6, 104.0, 121.0, 128.8, 132.4, 140.0, 156.3, 169.8, 181.5, 204.4; HRMS (FAB, mnba) calcd for $[C_{41}H_{59}N_3O_9 + H]^+$ 738.4330, found 738.4332.

Representative Procedure for the Synthesis of *O*-Trityl Protected Tricyclic Ketolide Hydroxamate. Tricyclic Ketolide-*N*-benzyltriazolyl-*O*-tritylhexahydroxamate (14a). 4-Ethynylbenzyltricyclic ketolide **9** (0.10 g, 0.14 mmol) and 6-azido-*O*-tritylhexahydroxamate **12a** (0.06 g, 0.14 mmol) were dissolved in anhydrous THF (7 mL) and stirred under argon at room temperature. Copper(I) iodide (0.012 g, 0.063 mmol) and Hunig's base (0.6 mL) were added to the reaction mixture, and stirring continued for 24 h. The reaction mixture was diluted with 1:4 NH_4OH/saturated NH_4Cl (50 mL) and extracted with 10% MeOH/CH_2Cl_2 (3 × 30 mL). The organic layers were combined, dried over Na_2SO_4, and concentrated in vacuo. The crude product was purified by preparative TLC (silica, 12:1:0.1 CH_2Cl_2/MeOH/conc NH_4OH) to give 127 mg (78%) of **14a** as a yellowish solid. ^{1}H NMR ($CDCl_3$, 400 MHz) δ 0.85 (3H, t, J = 7.6 Hz), 1.1 (3H, d, J = 6.8 Hz), 1.20−1.39 (17H, m), 1.46−2.00 (15H, m), 2.19 (3H, s), 2.58−2.80 (6H, m), 2.84−3.00 (1H, m), 3.02−3.17 (1H, m), 3.31−3.60 (3H, m), 3.64−3.87 (5H, m), 3.96−4.0 (1H, m), 4.22 (1H, d, J = 8.4 Hz), 4.29−4.32 (3H, m), 4.93 (1H, dd, J = 10.0, 1.6 Hz), 7.23−7.45 (17H, m), 7.71 (1H, s), 7.79 (2H, d, J = 8.0 Hz); ^{13}C NMR ($CDCl_3$, 100 MHz) δ 10.7, 11.1, 13.1, 14.6, 16.7, 19.3, 19.9, 21.4, 22.3, 22.8, 26.0, 29.6, 30.2, 31.0, 36.5, 37.0, 38.8, 42.5, 43.0, 48.3, 49.3, 49.7, 50.2, 51.4, 53.7, 57.7, 60.1, 65.6, 69.8, 70.5, 76.7, 78.7, 79.4, 81.8, 93.1, 104.1, 119.7, 126.0, 128.2, 128.4, 129.2, 129.4, 130.0, 138.9, 141.2, 147.6, 156.3, 169.8, 177.0, 181.5, 204.5; HRMS (ESI) calcd for $[C_{66}H_{85}N_7O_{11} + H]^+$ 1152.6379, found 1152.6367.

Tricyclic Ketolide-*N*-benzyltriazolyl-*O*-tritylheptahydroxamate (14b). Reaction of 4-ethynylbenzyltricyclic ketolide **9** (0.10 g, 0.14 mmol) and 7-azido-*O*-tritylheptahydroxamate **12b** (0.06 g, 0.14 mmol) within 24 h as described for the synthesis of **14a** gave 133 mg (83%) of **14b** as a yellowish solid. ^{1}H NMR ($CDCl_3$, 400 MHz) δ 0.85 (3H, t, J = 7.6 Hz), 1.06 (3H, d, J = 6.8 Hz), 1.20−1.42 (19H, m), 1.45−1.98 (15H, m), 2.20 (3H, s), 2.57−2.79 (6H, m), 2.85−3.00 (1H, m), 3.03−3.17 (1H, m), 3.30−3.57 (3H, m), 3.72−3.83 (5H, m), 3.96−4.00 (1H, m), 4.22 (1H, d, J = 8.8 Hz), 4.29−4.35 (3H, m), 4.95 (1H, dd, J = 10.4, 2.4 Hz), 7.22−7.45 (17H, m), 7.71 (1H, s), 7.78 (2H, d, J = 8.4 Hz); ^{13}C NMR ($CDCl_3$, 100 MHz) δ 10.7, 11.1, 13.1, 14.6, 16.6, 19.3, 19.9, 21.4, 22.3, 26.3, 29.6, 30.2, 36.5, 37.0, 38.8, 42.5, 43.0, 48.3, 49.3, 49.7, 50.4, 51.4, 53.7, 57.7, 60.1, 65.5, 69.7, 70.5, 76.7, 78.7, 79.4, 81.8, 92.8, 104.1, 119.7, 126.0, 128.4, 129.2, 129.4, 130.0, 132.3, 138.9, 141.3, 147.6, 156.3, 169.8, 177.6, 182.5, 204.5; HRMS (ESI) calcd for $[C_{67}H_{87}N_7O_{11} + H]^+$ 1166.6536, found 1166.6478.

Tricyclic Ketolide-*N*-benzyltriazolyl-*O*-trityloctahydroxamate (14c). Reaction of 4-ethynylbenzyltricyclic ketolide **9** (0.08 g, 0.10 mmol) and 8-azido-*O*-trityloctahydroxamate **12c** (0.05 g, 0.10 mmol) in anhydrous THF (5 mL) within 22 h as described for the synthesis of **14a** gave 94 mg (79%) of **14c** as a yellowish solid. ^{1}H NMR ($CDCl_3$, 400 MHz) δ 0.83 (3H, t, J = 7.2 Hz), 1.04 (3H, d, J = 7.2 Hz), 1.15−1.41 (21H, m), 1.45−1.95 (15H, m), 2.18 (3H, s), 2.55−2.73 (6H, m), 2.87−2.97 (1H, m), 3.03−3.10 (1H, m), 3.28−3.57 (3H, m), 3.70−3.82 (5H, m), 3.93−3.97 (1H, m), 4.21 (1H, d, J = 8.4 Hz), 4.27−4.34 (3H, m), 4.94 (1H, dd, J = 12.8, 2.4 Hz), 7.25−7.42 (17H, m), 7.71 (1H, s), 7.76 (2H, d, J = 8.0 Hz); ^{13}C NMR ($CDCl_3$, 100 MHz) δ 10.7, 11.1, 13.1, 14.6, 16.6, 19.3, 19.9, 21.4, 22.3, 26.4, 28.8, 29.6, 30.4, 36.6, 37.0, 38.8, 42.5, 42.9, 48.3, 49.3, 49.7, 50.6, 51.4, 53.7, 57.7, 60.1, 65.5, 69.8, 70.5, 76.7, 78.7, 79.4, 81.8, 93.8, 104.1, 119.6, 126.0, 127.7, 128.3, 128.8, 129.2, 129.4, 130.0, 132.7, 138.9, 141.3, 147.7, 156.3, 169.8, 177.0, 182.4, 204.4; HRMS (ESI) calcd for $[C_{68}H_{89}N_7O_{11} + H]^+$ 1180.6692, found 1180.6637.

Tricyclic Ketolide-*N*-benzyltriazolyl-*O*-tritylnonahydroxamate (14d). Reaction of 4-ethynylbenzyltricyclic ketolide **9** (0.08 g, 0.10 mmol) and 9-azido-*O*-tritylnonahydroxamate **12d** (0.05 g, 0.10 mmol) in anhydrous THF (5 mL) within 20 h as described for the synthesis of **14a** gave 93 mg (76%) of **14d** as a yellowish solid. ^{1}H NMR ($CDCl_3$, 400 MHz) δ 0.85 (3H, t, J = 8.0 Hz), 1.05 (3H, d, J = 6.8 Hz), 1.16−1.44 (23H, m), 1.45−1.96 (15H, m), 2.20 (3H, m), 2.57−2.78 (6H, m), 2.90−2.99 (1H, m), 3.02−3.12 (1H, m), 3.30−3.57 (3H, m), 3.72−3.84 (5H, m), 3.96−4.00 (1H, m), 4.29 (1H, d, J = 8.4 Hz), 4.31 (1H, d, J = 7.2 Hz), 4.37 (2H, t, J = 7.2 Hz), 4.95 (1H, dd, J = 12.8, 2.4 Hz), 7.19−7.45 (17H, m), 7.72 (1H, s), 7.78 (2H, d, J = 8.0 Hz); ^{13}C NMR ($CDCl_3$, 100 MHz) δ 10.7, 11.1, 13.1, 14.6, 16.6, 19.3, 19.9, 21.4, 22.3, 26.6, 28.9, 29.2, 29.6, 29.9, 30.5, 36.5, 37.0, 37.1, 38.8, 42.5, 43.0, 48.3, 49.3, 49.7, 50.6, 51.4, 57.7, 60.1, 65.5, 65.6, 69.7, 70.5, 76.7, 78.7, 79.4, 81.8, 94.3, 104.1, 119.6, 126.0, 128.3,

128.8, 129.0, 129.2, 129.4, 130.0, 132.3, 138.9, 141.3, 147.6, 156.3, 169.8, 178.0, 181.5, 204.5; HRMS (ESI) calcd for $[C_{69}H_{91}N_7O_{11} + H]^+$ 1194.6849, found 1194.6838.

Tricyclic Ketolide-*N*-benzyltriazolyl-*O*-trityldecahydroxamate (14e). Reaction of 4-ethynylbenzyltricyclic ketolide **9** (0.08 g, 0.10 mmol) and 10-azido-*O*-trityldecahydroxamate **12e** (0.05 g, 0.10 mmol) in anhydrous THF (5 mL) within 20 h as described for the synthesis of **14a** gave 98 mg (80%) of **14e** as a yellowish solid. ^{1}H NMR ($CDCl_3$, 400 MHz) δ 0.83 (3H, t, J = 6.8 Hz), 1.03 (3H, d, J = 7.2 Hz), 1.15−1.40 (25H, m), 1.44−1.96 (15H, m), 2.17 (3H, s), 2.57−2.78 (6H, m), 2.87−2.95 (1H, m), 3.03−3.08 (1H, m), 3.28−3.53 (3H, m), 3.70−3.82 (5H, m), 3.92−3.96 (1H, m), 4.20 (1H, d, J = 8.4 Hz), 4.29 (1H, d, J = 6.8 Hz), 4.33 (2H, t, J = 7.2 Hz), 4.93 (1H, d, J = 10.0 Hz), 7.26−7.43 (17H, m), 7.73 (1H, s), 7.76 (2H, d, J = 8.0 Hz); ^{13}C NMR ($CDCl_3$, 100 MHz) δ 10.7, 11.1, 13.1, 14.6, 16.6, 19.3, 19.8, 21.4, 22.3, 26.6, 29.1, 29.3, 29.6, 29.9, 30.5, 36.6, 37.0, 38.8, 42.5, 43.0, 48.3, 49.3, 49.7, 50.6, 51.4, 57.7, 60.1, 65.5, 69.7, 70.5, 76.7, 78.7, 79.4, 81.8, 93.4, 104.1, 199.6, 126.0, 128.3, 129.2, 129.4, 130.0, 138,9, 147.6, 156.3, 169.8, 177.6, 182.0, 204.5; HRMS (ESI) calcd for $[C_{70}H_{93}N_7O_{11} + H]^+$ 1208.7005, found 1208.6888.

Tricyclic Ketolide-*N*-benzyltriazolylhexahydroxamic Acid (15a). Method A. To a solution of **14a** (0.12 g, 0.11 mmol) in methylene chloride (1 mL) at 0 °C was added thioanisole (0.2 mL) and TFA (0.2 mL) dropwise. Stirring was continued at 0 °C for 2 h, after which TLC analysis indicated complete consumption of the starting material. Excess TFA and solvent were evaporated off, and the residue was immediately placed in an ice bath followed by addition of PBS buffer (10 mL). Saturated $NaHCO_3$ was added dropwise until the pH was neutral. Extraction with 20% MeOH/CH_2Cl_2 (10 mL × 3), drying over Na_2SO_4, and evaporation of solvent afforded crude product which was then purified by preparative TLC (silica, 12:1:0.1 CH_2Cl_2/MeOH/conc NH_4OH) to afford 47 mg (50%) of **15a** as a yellow-white solid.

Method B. To a mixture of **14a** (0.14 g, 0.12 mmol) in CH_2Cl_2/MeOH (2 mL/2 mL) was added $BF_3 \cdot OEt_2$ (0.03 g, 0.24 mmol), and the mixture was stirred at room temperature for 45 min. Dilute $NaHCO_3$ was added until pH 8 was obtained (approximately 20 mL), and the suspension was extracted with 10% MeOH/CH_2Cl_2 (10 mL ×x 4), dried over Na_2SO_4, and concentrated in vacuo. The crude product was purified by preparative TLC (silica, 12:1:0.1 CH_2Cl_2/MeOH/conc NH_4OH) to give 64 mg (60%) of **15a** as a yellow-white solid.

Method C. 4-Ethynylbenzyltricyclic ketolide **9** (0.05 g, 0.07 mmol) and 6-azidohexahydroxamic acid[24] **13a** (0.03 g, 0.15 mmol) were dissolved in anhydrous THF (7 mL) with stirring under argon at room temperature. Copper(I) iodide (0.01 g, 0.04 mmol) and Hunig's base (0.5 mL) were added to the reaction mixture, and stirring continued for 12 h. The reaction mixture was diluted with 10% MeOH/CH_2Cl_2 (20 mL) and washed with 1:4 NH_4OH/saturated NH_4Cl (3 × 10 mL) and saturated NH_4Cl (10 mL). The organic layer was dried over Na_2SO_4 and concentrated in vacuo. The crude product was purified by preparative TLC (silica, 12:1:0.1 CH_2Cl_2/MeOH/conc NH_4OH) to give 20 mg (34%) of **15a** as a brown-white solid. Mp 127−130 °C; retention time 20.167 min; ^{1}H NMR ($CDCl_3$, 400 MHz) δ 0.85 (3H, t, J = 8.0 Hz), 1.05 (3H, d, J = 7.2 Hz), 1.20−2.00 (30H, m), 2.13−2.18 (2H, m), 2.20 (3H, s), 2.58−2.72 (6H, m), 2.92−2.98 (1H, m), 3.05−3.09 (1H, m), 3.30−3.55 (3H, m), 3.70−3.84 (5H, m), 3.95−3.98 (1H, m), 4.22 (1H, d, J = 8.0 Hz), 4.31−4.38 (3H, m), 4.95 (1H, d, J = 8.8 Hz), 7.33 (2H, d, J = 8.0 Hz), 7.77 (3H, m); ^{13}C NMR ($CDCl_3$, 100 MHz) δ 10.6, 11.1, 13.1, 14.6, 16.5, 19.3, 19.8, 21.4, 22.3, 24.7, 25.9, 29.7, 29.9, 30.0, 36.6, 37.1, 38.8, 42.5, 42.8, 49.4, 49.6, 50.3, 51.4, 53.7, 57.7, 60.1, 65.5, 69.7, 70.5, 76.7, 78.7, 79.3, 81.8, 104.1, 120.1, 126.0, 129.5, 129.7, 139.1, 147.7, 156.3, 169.8, 171.1, 182.3, 204.5; HRMS (ESI) calcd for $[C_{47}H_{71}N_7O_{11} + H]^+$ 910.5284, found 910.5279.

Tricyclic Ketolide-*N*-benzyltriazolylheptahydroxamic Acid (15b). The reaction of **14b** (0.13 g, 0.11 mmol) in CH_2Cl_2 (1 mL), thioanisole (0.3 mL), and TFA (0.3 mL), according to method A, for 3 h afforded 56 mg (55%) of **15b** as a yellow-white solid.

Similarly, the reaction of **14b** (0.15 g, 0.18 mmol) and $BF_3 \cdot OEt_2$ (0.04 g, 0.26 mmol), according to method B, afforded 65 mg (55%) of **15b** as a yellow-white solid.

Also, the reaction of 4-ethynylbenzyltricyclic ketolide **9** (0.05 g, 0.06 mmol) and 7-azidoheptahydroxamic acid **13b** (0.02 g, 0.11 mmol) within 12 h, according, to method C, gave 22 mg (38%) of **15b** as a brown-white solid. Mp 128−131 °C; retention time 21.233 min; ^{1}H NMR ($CDCl_3$, 400 MHz) δ 0.83 (3H, t, J = 7.6 Hz), 1.03 (3H, d, J = 6.4 Hz), 1.18−1.90 (32H, m), 2.10−2.13 (2H, m), 2.17 (3H, s), 2.58−2.73 (6H, m), 2.93−2.98 (1H, m), 3.03−3.07 (1H, m), 3.28−3.60 (3H, m), 3.70−3.81 (5H, m), 3.98 (1H, m), 4.20 (1H, d, J = 8.4 Hz), 4.29−4.38 (3H, m), 4.93 (1H, d, J = 10.4 Hz), 7.30 (2H, d, J = 7.6 Hz), 7.75 (2H, d, J = 7.6 Hz), 7.78 (1H, s); ^{13}C NMR ($CDCl_3$, 100 MHz) δ 10.6, 11.1, 13.1, 14.6, 16.5, 19.3, 19.8, 21.4, 22.3, 25.2, 26.0, 28.2, 29.7, 29.9, 30.1, 36.6, 37.0, 38.8, 42.5, 42.7, 48.2, 49.3, 49.5, 50.4, 51.4, 53.7, 57.7, 60.1, 65.5, 69.7, 70.5, 76.7, 78.7, 79.3, 81.8, 104.0, 120.0, 126.0, 129.4, 129.8, 139.1, 147.7, 156.3, 169.8, 171.2, 182.4, 204.5; HRMS (ESI) calcd for $[C_{48}H_{73}N_7O_{11} + H]^+$ 924.5440, found 924.5422.

Tricyclic Ketolide-*N*-benzyltriazolyloctahydroxamic Acid (15c). The reaction of **14c** (0.09 g, 0.08 mmol) in CH_2Cl_2 (1 mL), thioanisole (0.2 mL), and TFA (0.2 mL), according to method A, afforded 37 mg (51%) of **15c** as a yellow-white solid. Mp 113−115 °C; retention time 22.533 min; ^{1}H NMR ($CDCl_3$, 400 MHz) δ 0.83 (3H, t, J = 6.4 Hz), 1.03 (3H, d, J = 5.6 Hz), 1.18−1.60 (21H, m), 1.66−2.1 (15H, m), 2.18 (3H, s), 2.56−2.70 (6H, m), 2.90−2.98 (1H, m), 3.02−3.07 (1H, m), 3.28−3.58 (3H, m), 3.70−3.81 (5H, m), 3.94−3.97 (1H, m), 4.20 (1H, d, J = 7.2 Hz), 4.28 (1H, d, J = 6.0 Hz), 4.35 (2H, m), 4.93 (1H, d, J = 10.4 Hz), 7.30 (2H, d, J = 7.2 Hz), 7.73−7.76 (3H, m); ^{13}C NMR ($CDCl_3$, 100 MHz) δ 10.6, 11.1, 13.1, 14.4, 14.6, 16.5, 19.3, 19.8, 21.3, 21.4, 22.3, 25.2, 26.1, 28.3, 29.7, 29.9, 30.2, 32.9, 36.6, 37.1, 38.8, 42.5, 42.7, 48.2, 49.4, 49.5, 50.5, 51.4, 57.7, 60.1, 60.6, 65.5, 69.7, 70.5, 76.7, 78.7, 79.3, 81.8, 104.0, 119.9, 126.0, 129.5, 129.8, 139.0, 147.7, 156.3, 169.8, 171.7, 182.4, 204.5; HRMS (ESI) calcd for $[C_{49}H_{75}N_7O_{11} + H]^+$ 938.5597, found 938.5556.

Tricyclic Ketolide-*N*-benzyltriazolylnonahydroxamic Acid (15d). The reaction of **14d** (0.09 g, 0.08 mmol) in CH_2Cl_2 (1 mL), thioanisole (0.2 mL), and TFA (0.2 mL), according to method A, afforded 43 mg (60%) of **15d** as a yellow-white solid. Mp 112−115 °C; retention time 23.983 min; ^{1}H NMR ($CDCl_3$, 400 MHz) δ 0.83 (3H, t, J = 7.2 Hz), 1.03 (3H, d, J = 7.2 Hz), 1.17−1.60 (23H, m), 1.66−2.14 (15H, m), 2.17 (3H, s), 2.58−2.73 (6H, m), 2.87−2.95 (1H, m), 3.00−3.07 (1H, m), 3.27−3.55 (3H, m), 3.70−3.82 (5H, m), 3.93−3.97 (1H, m), 4.20 (1H, d, J = 8.8 Hz), 4.28 (1H, d, J = 7.2 Hz), 4.35 (2H, t, J = 6.8 Hz), 4.92 (1H, dd, J = 10.0, 1.2 Hz), 7.30 (2H, d, J = 8.0 Hz), 7.75 (3H, m); ^{13}C NMR ($CDCl_3$, 100 MHz) δ 10.7, 11.1, 13.1, 14.6, 16.5, 19.3, 19.8, 21.4, 22.3, 25.4, 26.3, 28.6, 28.8, 28.9, 29.6, 29.9, 30.3, 32.9, 36.6, 37.1, 38.8, 42.5, 42.8, 48.2, 49.3, 49.6, 50.6, 51.4, 57.7, 60.1, 65.5, 69.7, 70.5, 76.7, 78.7, 79.3, 81.8, 104.1, 119.8, 126.0, 129.5, 129.8, 139.0, 147.7, 156.3, 169.8, 171.3, 182.9, 204.5; HRMS (ESI) calcd for $[C_{50}H_{77}N_7O_{11} + H]^+$ 952.5753, found 952.5728.

Tricyclic Ketolide-*N*-benzyltriazolyldecahydroxamic Acid (15e). The reaction of **14e** (0.10 g, 0.08 mmol) in CH_2Cl_2 (1 mL), thioanisole (0.2 mL), and TFA (0.2 mL), according to method A, afforded 42 mg (55%) of **15e** as a yellow-white solid. Mp 123−126 °C; retention time 25.583 min; ^{1}H NMR ($CDCl_3$, 400 MHz) δ 0.83 (3H, t, J = 7.2 Hz), 1.03 (3H, d, J = 6.4 Hz), 1.18−1.61 (25H, m), 1.66−2.14 (15H, m), 2.18 (3H, s), 2.59−2.73 (6H, m), 2.89−2.94 (1H, m), 3.01−3.07 (1H, m), 3.28−3.54 (3H, m), 3.70−8.83 (5H, m), 3.93−3.97 (1H, m), 4.20 (1H, d, J = 8.4 Hz), 4.28 (1H, d, J = 6.8 Hz), 4.36 (2H, t, J = 7.2 Hz), 4.92 (1H, dd, J = 10.4, 1.6 Hz), 7.30 (2H, d, J = 8.0 Hz), 7.76 (3H, m); ^{13}C NMR ($CDCl_3$, 100 MHz) δ 10.7, 11.1, 13.1, 14.4, 14.6, 16.5, 19.3, 19.9, 21.4, 22.3, 25.5, 26.3, 28.7, 28.9, 29.0,

29.6, 29.9, 30.3, 33.1, 36.6, 37.1, 38.8, 42.5, 42.7, 48.2, 49.4, 49.5, 50.6, 51.4, 57.7, 60.1, 60.6, 65.5, 69.7, 70.5, 76.7, 78.7, 79.3, 81.8, 104.0, 119.8, 126.0, 129.5, 129.8, 139.0, 147.7, 156.3, 169.8, 171.7, 182.9, 204.5; HRMS (ESI) calcd for $[C_{51}H_{79}N_7O_{11} + H]^+$ 966.5910, found 966.5919.

Biological Assays. In Vitro HDAC Inhibition. (a) Fluorescence Assay. In vitro activity against HeLa nuclear extract was determined as previously described.[24,32,45] Briefly, 15 μL of HeLa nuclear extract was mixed with 5 μL of 10× compound and 5 μL of assay buffer. Fluorogenic substrate (25 μL) was added, and mixture was allowed to proceed for 15 min at room temperature and then stopped by addition of a developer containing TSA. Fluorescence was monitored after 15 min at excitation and emission wavelengths of 360 and 460 nm, respectively. Assays against HDAC8 and HDAC6 were performed according to the manufacturer's instructions.

(b) SAMDI Assay. The maleimide-presenting SAMs and expression of HDAC8 enzyme were prepared as previously reported.[41] The peptide substrate (Ac-GRK^{Ac}FGC-NH_2) was synthesized using standard FMOC solid phase peptide synthesis protocols using reagents from Anaspec (San Jose, CA). The enzyme was diluted to 1 μM in buffer (25 mM Tris-HCl (pH 8.0) containing 137 mM NaCl, 2.7 mM KCl, and 1 mM $MgCl_2$) with varying concentrations of inhibitor (0, 50, 100, 250, and 500 nM) for 5 min at room temperature. The reaction was initiated upon substrate addition (5, 10, 25, and 50 μM) to a final volume of 20 μL per reaction, and the plate was incubated at 37 °C. At each time point (0, 3, 6, 9, and 12 min), 3 μL aliquots were transferred to a separate plate, and the reaction was terminated by heating to 80 °C for 1 min. After collection of all time points, the aliquots were transferred to the maleimide-presenting arrays and incubated at 37 °C for 1 h to allow the immobilization of the peptide substrate. The arrays were then washed with water, ethanol and dried under nitrogen. Matrix (2,4,6-trihydroxyacetophenone, 0.01 μL, 20 mg/mL in acetone) was applied, air-dried, and the arrays were analyzed by SAMDI MS.

(c) Pf-HDAC1 Inhibition Studies. These were performed as described in ref 47.

Mass Spectrometry and Data Analysis. Mass analysis was performed using an Applied Biosystems 4800 MALDI TOF/TOF mass spectrometer (Framingham, MA). A 355 nm Nd:YAG laser was used as a desorption ionization source, and all spectra were acquired with 20 kV accelerating voltage in positive reflector mode. The extent of reaction was calculated as previously reported.[41] Briefly, the relative amount of each compound was calculated by measuring the relative peak intensities of each molecular ion peak (M^+) [amount of $X = I_x/(I_x + I_y)$] where x refers to the deacetylated peak and y is the parent ion. For K_i analysis, the micromoles of deacetylated peptide were plotted over time and the slope of the linear portion was measured to give the initial velocity of the reaction. A Dixon plot was then created ([I] vs $1/v$), and the intersecting point corresponds to the K_i of the inhibitor.

Cell Growth Inhibition. All cell lines were maintained in a 37 °C environment containing 5% CO_2 with recommended media (ATCC). For cell growth inhibition, cells were passaged the day before dosing into a 96-well cell culture plate and allowed to grow for a minimum of 24 h prior to drug addition. All compounds were diluted first to 1000× test concentration in DMSO and then to test concentrations in cell media so that the DMSO concentration would be constant across all wells at 0.1% in a 100 μL volume. Cells were dosed for 72 h, and then 20 μL of MTS reagent was added and allowed to incubate for 2 h. Absorbance was then determined using an absorbance plate reader set to 490 nm.

Antimalarial and Antileishmanial Assays. In vitro antimalarial and antileishmanial activities were determined as previously described.[46] Briefly, antimalarial activity of the compounds was determined in vitro on chloroquine sensitive (D6, Sierra Leone) and resistant (W2, IndoChina) strains of *Plasmodium falciparum*. The 96-well microplate assay is based on evaluation of the effect of the compounds on growth of asynchronous cultures of *P. falciparum*, determined by the assay of parasite lactate dehydrogenase (pLDH) activity.[53] The appropriate dilutions of the compounds were prepared in DMSO or RPMI-1640 medium and added to the cultures of *P. falciparum* (2% hematocrit, 2% parasitemia) set up in clear flat-bottomed 96-well plates. The plates were placed into a humidified chamber and flushed with a gas mixture of 90% N_2, 5% CO_2, and 5% O_2. The cultures were incubated at 37 °C for 72 h. Growth of the parasite in each well was determined by pLDH assay using Malstat reagent.[53] The medium and RBC controls were also set up in each plate. The standard antimalarial agents, chloroquine and artemisinin, were used as the positive controls, while DMSO was tested as the negative control. Antileishmanial activity of the compounds was tested in vitro on a culture of *Leishmania donovani* promastigotes. In a 96-well microplate assay, compounds with appropriate dilution were added to the leishmania promastigotes culture (2×10^6 cell/mL). The plates were incubated at 26 °C for 72 h, and growth of leishmania promastigotes was determined by Alamar blue assay.[54] Pentamidine and amphotericin B were tested as standard antileishmanial agents. All the compounds were simultaneously tested for cytotoxicty on VERO (monkey kidney epithilial) cells by Neutral Red assay.[55] The IC_{50} value for each compound was computed from the growth inhibition curve.

Acknowledgment. This work was financially supported by Georgia Institute of Technology, by the Blanchard fellowship, and by NIH Grant R01CA131217 (A.K.O.). National Center for Natural Products Research is partially supported by USDA-ARS Scientific Cooperative Agreement No. 58-6408-2-0009. W.G. is a recipient of a GAANN predoctoral fellowship from the Georgia Tech Center for Drug Design, Development, and Delivery. Z.A.G.-L. is supported by the ARCS Foundation Chicago Chapter. M.M. is supported by NIH Grant RO1 GM084188.

Supporting Information Available: ^{1}H NMR and ^{13}C NMR spectral information, HPLC traces, and pf-HDAC1 activity dose-response curves of **15a**−**e** and molecular modeling outputs. This material is available free of charge via the Internet at http://pubs.acs.org.

References

(1) Jenuwein, T.; Allis, C. D. Translating the histone code. *Science* **2001**, *293* (5532), 1074–1080.
(2) Johnstone, R. W. Histone-deacetylase inhibitors: novel drugs for the treatment of cancer. *Nat. Rev. Drug Discovery* **2002**, *1* (4), 287–299.
(3) Bolden, J. E.; Peart, M. J.; Johnstone, R. W. Anticancer activities of histone deacetylase inhibitors. *Nat. Rev. Drug Discovery* **2006**, *5* (9), 755–768.
(4) Somech, R.; Izraeli, S.; Simon, A. J. Histone deacetylase inhibitors—a new tool to treat cancer. *Cancer Treat. Rev.* **2004**, *30* (5), 461–472.
(5) Boyes, J.; Byfield, P.; Nakatani, Y.; Ogryzko, V. Regulation of activity of the transcription factor GATA-1 by acetylation. *Nature* **1998**, *396* (6711), 594–598.
(6) Gu, W.; Roeder, R. G. Activation of p53 sequence-specific DNA binding by acetylation of the p53 C-terminal domain. *Cell* **1997**, *90* (4), 595–606.
(7) Jin, S.; Scotto, K. W. Transcriptional regulation of the MDR1 gene by histone acetyltransferase and deacetylase is mediated by NF-Y. *Mol. Cell. Biol.* **1998**, *18* (7), 4377–4384.
(8) Vigushin, D. M.; Coombes, R. C. Targeted Histone deacetylase inhibition for cancer therapy. *Curr. Cancer Drug Targets* **2004**, *4* (2), 205–218.
(9) Yang, X.-J.; Seto, E. The Rpd3/Hda1 family of lysine deacetylases: from bacteria and yeast to mice and men. *Nat. Rev. Mol. Cell Biol.* **2008**, *9* (3), 206–218.
(10) Choudhary, C.; Kumar, C.; Gnad, F.; Nielsen, M. L.; Rehman, M.; Walther, T. C.; Olsen, J. V.; Mann, M. Lysine acetylation targets

protein complexes and co-regulates major cellular functions. *Science* **2009**, *325* (5942), 834–840.
(11) Zhang, Y.; Fang, H.; Jiao, J.; Xu, W. The structure and function of histone deacetylases: the target for anti-cancer therapy. *Curr. Med. Chem.* **2008**, *15* (27), 2840–2849.
(12) Neugebauer, R. C.; Sippl, W.; Jung, M. Inhibitors of NAD^+ dependent histone deacetylases (sirtuins). *Curr. Pharm. Des.* **2008**, *14* (6), 562–573.
(13) Kelly, W. K.; O'Connor, O. A.; Marks, P. A. Histone deacetylase inhibitors: from target to clinical trials. *Expert Opin. Invest. Drugs* **2002**, *11*, 1695–1713.
(14) Miller, T. A.; Witter, D. J.; Belvedere, S. Histone deacetylase inhibitors. *J. Med. Chem.* **2003**, *46* (24), 5097–5116.
(15) Grant, S.; Easley, C.; Kirkpatrick, P. Vorinostat. *Nat. Rev. Drug Discovery* **2007**, *6* (1), 21–22.
(16) http://www.fda.gov/cder/Offices/OODP/whatsnew/vorinostat.htm.
(17) http://www.medicalnewstoday.com/articles/170146.php.
(18) http://www.celgene.com/utility/celgene-inter.aspx?source=product&display=www.istodax.com&exit_url=www.istodax.com.
(19) Al-Janadi, A.; Chandana, S. R.; Conley, B. A. Histone deacetylation: an attractive target for cancer therapy? *Drugs R&D* **2008**, *9* (6), 369–383.
(20) Jones, P.; Steinkühler, C. From natural products to small molecule ketone histone deacetylase inhibitors: development of new class specific agents. *Curr. Pharm. Des.* **2008**, *14* (6), 545–561.
(21) Itoh, Y.; Suzuki, T.; Miyata, N. Isoform-selective histone deacetylase inhibitors. *Curr. Pharm. Des.* **2008**, *14* (6), 529–544.
(22) Bieliauskas, A. V.; Pflum, M. K. H. Isoform-selective histone deacetylase inhibitors. *Chem. Soc. Rev.* **2008**, *37*, 1402–1413.
(23) http://www.clinicaltrials.gov/ct/show/NCT00106431.
(24) Oyelere, A. K.; Chen, P. C.; Guerrant, W.; Mwakwari, S. C.; Hood, R.; Zhang, Y.; Fan, Y. Non-peptide macrocyclic histone deacetylase inhibitors. *J. Med. Chem.* **2009**, *52*, 456–468.
(25) Kashimura, M.; Asaka, T.; Misawa, Y.; Matsumoto, K.; Morimoto, S. Synthesis and antibacterial activity of the tricyclic ketolides TE-802 and its analogs. *J. Antibiot.* **2001**, *54* (8), 664–678.
(26) Plata, D. J.; Leanna, M. R.; Rasmussen, M.; McLaughlin, M. A.; Condon, S. L.; Kerdesky, F. A. J.; King, S. A.; Peterson, M. J.; Stoner, E. J.; Wittenberger, S. J. The synthesis of ketolide antibiotic ABT-773 (cethromycin). *Tetrahedron* **2004**, *60* (45), 10171–10180.
(27) Beebe, X.; Yang, F.; Bui, M. H.; Mitten, M. J.; Ma, Z.; Nilius, A. M.; Djuric, S. W. Synthesis and antibacterial activity of 6-*O*-arylpropargyl-9-oxime-11,12-carbamate ketolides. *Bioorg. Med. Chem. Lett.* **2004**, *14* (10), 2417–2421.
(28) Estiu, G.; Wiest, O. HDAC1 homology model. Personal communication.
(29) Randolph, o. T.; Waid, P.; Nichols, C.; Sauer, D.; Haviv, F.; Diaz, G.; Bammert, G.; Besecke, L. M.; Segreti, J. A.; Mohning, K. M.; Bush, E. N.; Wegner, C. D.; Greer, J. Nonpeptide luteinizing hormone-releasing hormone antagonists derived from erythromycin A: design, synthesis, and biological activity of cladinose replacement analogues. *J. Med. Chem.* **2004**, *47* (5), 1085–1097.
(30) Agouridas, C.; Denis, A.; Auger, J.-M.; Benedetti, Y.; Bonnefoy, A.; Bretin, F.; Chantot, J.-F.; Dussarat, A.; Fromentin, C.; D'Ambrières, S. G.; Lachaud, S.; Laurin, P.; Martret, O. L.; Loyau, V.; Tessot, N. Synthesis and antibacterial activity of ketolides (6-*O*-methyl-3-oxoerythromycin derivatives): a new class of antibacterials highly potent against macrolide-resistant and -susceptible respiratory pathogens. *J. Med. Chem.* **1998**, *41* (21), 4080–4100.
(31) Denis, A.; Renou, C. Novel N-demethylation of ketolide: application to the solution phase parallel synthesis of *N*-desosaminyl-substituted ketolides using ion exchange resins. *Tetrahedron Lett.* **2002**, *43* (23), 4171–4174.
(32) *HDAC Fluorimetric Assay/Drug Discovery Kit. AK-500 Manual. Fluorescent Assay System*; ENZO Life Sciences International, Inc.: Plymouth Meeting, PA, 2009.
(33) *HDAC 8 Fluorimetric Drug Discovery Kit. AK-518 Manual*; ENZO Life Sciences International, Inc.: Plymouth Meeting, PA, 2009.
(34) *HDAC 6. SE-508 Manual*; ENZO Life Sciences International, Inc.: Plymouth Meeting, PA, 2009.
(35) Somoza, J. R.; Skene, R. J.; Katz, B. A.; Mol, C.; Ho, J. D.; Jennings, A. J.; Luong, C.; Arvai, A.; Buggy, J. J.; Chi, E.; Tang, J.; Sang, B.-C.; Verner, E.; Wynands, R.; Leahy, E. M.; Dougan, D. R.; Snell, G.; Navre, M.; Knuth, M. W.; Swanson, R. V.; McRee, D. E.; Tari, L. W. Structural snapshots of human HDAC8 provide insights into the class I histone deacetylases. *Structure* **2004**, *12*, 1325–1334.
(36) KrennHrubec, K.; Marshall, B. L.; Hedglin, M.; Verdin, E.; Ulrich, S. M. Design and evaluation of "linkerless" hydroxamic acids as selective HDAC8 inhibitors. *Bioorg. Med. Chem. Lett.* **2007**, *17*, 2874–2878.
(37) Borra, M. T.; Smith, B. C.; Denu, J. M. Mechanism of human SIRT1 activation by resveratrol. *J. Biol. Chem.* **2005**, *280* (17), 17187–17195.
(38) Kaeberlein, M.; McDonagh, T.; Heltweg, B.; Hixon, J.; Westman, E. A.; Caldwell, S. D.; Napper, A.; Curtis, R.; DiStefano, P. S.; Fields, S.; Bedalov, A.; Kennedy, B. K. Substrate-specific activation of sirtuins by resveratrol. *J. Biol. Chem.* **2005**, *280* (17), 17038–17045.
(39) Pacholec, M.; Bleasdale, J. E.; Chrunyk, B.; Cunningham, D.; Flynn, D.; Garofalo, R. S.; Griffith, D.; Griffor, M.; Loulakis, P.; Pabst, B.; Qiu, X.; Stockman, B.; Thanabal, V.; Varghese, A.; Ward, J.; Withka, J.; Ahn, K. SRT1720, SRT2183, SRT1460, and resveratrol are not direct activators of SIRT1. *J. Biol. Chem.* **2010**, *285* (11), 8340–8351.
(40) Beher, D.; Wu, J.; Cumine, S.; Kim, K. W.; Lu, S.-C.; Atangan, L.; Wang, M. Resveratrol is not a direct activator of SIRT1 enzyme activity. *Chem. Biol. Drug Des.* **2009**, *74* (6), 619–624.
(41) Gurard-Levin, Z. A.; Kim, J.; Mrksich, M. Combining mass spectrometry and peptide arrays to profile the specificities of histone deacetylases. *ChemBioChem* **2009**, *10* (13), 2159–2161.
(42) Mrksich, M. Mass spectrometry of self-assembled monolayers: a new tool for molecular surface science. *ACS Nano* **2008**, *2* (1), 7–18.
(43) Gurard-Levin, Z. A.; Mrksich, M. The activity of HDAC8 depends on local and distal sequences of its peptide substrates. *Biochemistry* **2008**, *47* (23), 6242–6250.
(44) Min, D.-H.; Yeo, W.-S.; Mrksich, M. A method for connecting solution-phase enzyme activity assays with immobilized format analysis by mass spectrometry. *Anal. Chem.* **2004**, *76* (14), 3923–3929.
(45) Chen, P. C.; Patil, V.; Guerrant, W.; Green, P.; Oyelere, A. K. Synthesis and structure−activity relationship of histone deacetylase (HDAC) inhibitors with triazole-linked cap group. *Bioorg. Med. Chem.* **2008**, *16* (9), 4839–4853.
(46) Patil, V.; Guerrant, W.; Chen, P. C.; Gryder, B.; Benicewicz, D. B.; I.Khan, S.; Tekwani, B. L.; Oyelere, A. K. Antimalarial and antileishmanial activities of histone deacetylase inhibitors with triazole-linked cap group. *Bioorg. Med. Chem.* **2010**, *18* (1), 415–425.
(47) Andrews, K. T.; Tran, T. N.; Lucke, A. J.; Kahnberg, P.; Le, G. T.; Boyle, G. M.; Gardiner, D. L.; Skinner-Adams, T. S.; Fairlie, D. P. Potent antimalarial activity of histone deacetylase inhibitor analogues. *Antimicrob. Agents Chemother.* **2008**, *52*, 1454–1461.
(48) Agbor-Enoh, S.; Seudieu, C.; Davidson, E.; Dritschilo, A.; Jung, M. Novel inhibitor of Plasmodium histone deacetylase that cures *P. berghei*-infected mice. *Antimicrob. Agents Chemother.* **2009**, *53*, 1727–1734.
(49) Dow, G. S.; Chen, Y.; Andrews, K. T.; Caridha, D.; Gerena, L.; Gettayacamin, M.; Johnson, J.; Melendez, V.; Obaldia, N., III; Tran, T. N.; Kozikowski, A. P. Antimalarial activity of phenylthiazolyly-bearing hydroxamate-based histone deacetylase inhibitors. *Antimicrob. Agents Chemother.* **2008**, *52*, 3467–3477.
(50) Guerrant, W.; Mwakwari, S. C.; Chen, P. C.; Khan, S. I.; Tekwani, B. L.; Oyelere, A. K. A structure activity relationship study of the antimalarial and antileishmanial activities of nonpeptide macrocyclic histone deacetylase inhibitors. *ChemMedChem* **2010**, *5*, 1232–1235.
(51) Bosnar, M.; Kelneric, Z.; Munic, V.; Erakovic, V.; Parnham, M. J. Cellular uptake and efflux of azithromycin, erythromycin, clarithromycin, telithromycin, and cethromycin. *Antimicrob. Agents Chemother.* **2005**, *49* (6), 2372–2377.
(52) Lugrin, J.; Ding, X. C.; Le Roy, D.; Chanson, A.-L.; Sweep, F. C.; Calandra, T.; Roger, T. Histone deacetylase inhibitors repress macrophage migration inhibitory factor (MIF) expression by targeting MIF gene transcription through a local chromatin deacetylation. *Biochim. Biophys. Acta, Mol. Cell Res.* **2009**, *1793* (11), 1749–1758.
(53) Makler, M. T.; Ries, J. M.; Williams, J. A.; Bancroft, J. E.; Piper, R. C.; Gibbins, B. L.; Hinriches, D. J. Parasite lactate dehydrogenase as an assay for *Plasmodium falciparum* drug sensitivity. *Am. J. Trop. Med. Hyg.* **1993**, *48* (6), 742–747.
(54) Mikus, J.; Steverding, D. A simple colorimetric method to screen drug cytotoxicity against Leishmania using the dye Alamar Blue. *Parasitol. Int.* **2009**, *48* (3), 265–269.
(55) Babich, H.; Borenfreund, E. Cytotoxicity of T-2 toxin and its metabolites determined with the neutral red cell viability assay. *Appl. Environ. Microbiol.* **1991**, *57* (7), 2101–2103.